

Piezoelectric Bimorph Actuator With Integrated Strain Sensing Electrodes

Sepehr Zarif Mansour¹, Rudolf J. Seethaler, *Member, IEEE*, Yik R. Teo, Yuen Kuan Yong²,
and Andrew J. Fleming³

Abstract—This paper describes a new method for estimating the tip displacement of piezoelectric benders. Two resistive strain gauges are fabricated within the top and bottom electrodes using an acid etching process. These strain gauges are employed in a half bridge electrical configuration to measure the surface resistance change, and estimate the tip displacement. Experimental validation shows a 1.1% maximum difference between the strain sensor and a laser triangulation sensor. Using the presented method, a damping-integral control structure is designed to control the tip displacement of the integrated bender.

Index Terms—Piezoelectric actuators, strain measurement, displacement control.

I. INTRODUCTION

PIEZOELECTRIC actuators are used in a wide range of positioning applications such as micro-manipulating [1], vibration control [2], and Atomic Force Microscopy [3]. Piezoelectric benders are a sub-type that are widely used in industrial and commercial applications. [4]. Bender actuators can primarily be classified as either pinned benders or bonded benders. Disk benders are an example of a pinned type bender [5], [6]. They consist of one or two circular piezoelectric elements glued to a non-piezoelectric layer. The outer edge of the disk is pinned to a stationary base while an electric field is applied to the bender developing a net displacement and force at the center of the disk.

Unimorph and bimorph benders are examples of bonded type benders [4], [7]. Unimorph benders have one piezoelectric plate bonded to a non-piezoelectric layer. Bimorph benders, which are employed in this study, consist of two piezoelectric plates that are bonded together. In order to provide reinforcement, a third elastic plate is sandwiched between the piezoelectric plates. In the cantilever configuration, an electric field is applied so that one plate expands while the other one contracts, which develops a net force and displacement at the tip.

Control of the tip displacement is a challenging task due to the lightly damped resonance and hysteresis [7], [8].

Manuscript received April 30, 2018; accepted May 25, 2018. Date of publication May 30, 2018; date of current version June 26, 2018. This work was supported by the Australian Research Council. The associate editor coordinating the review of this paper and approving it for publication was Prof. Subhas C. Mukhopadhyay. (*Corresponding author: Sepehr Zarif Mansour.*)

S. Zarif Mansour and R. J. Seethaler are with The University of British Columbia, Kelowna, BC V1V 1V7, Canada (e-mail: sepehr.zmansour@alumni.ubc.ca).

Y. R. Teo, Y. K. Yong, and A. J. Fleming are with the Precision Mechatronics Laboratory, The University of Newcastle, Callaghan, NSW 2308, Australia. Digital Object Identifier 10.1109/JSEN.2018.2842138

Feedback control techniques such as, positive position feedback [9], damping-integral control [10], and integral resonant control [11], measure the tip displacement using an external displacement sensor. The displacement can also be estimated by bonding a strain gauge to the actuator surface, which is attractive due to the small form factor and low cost. Strain gauges can be used as displacement sensors for controlling piezoelectric stack actuators [12].

This article¹ describes a new method for measuring the tip displacement of piezoelectric benders by integrating strain sensors into the top and bottom electrodes. The surface strain is shown to be directly proportional to the tip displacement. The strain gauges are configured in a half bridge circuit which requires a bipolar excitation and avoids the need for an instrumentation amplifier. The performance of the proposed method is validated by employing the integrated bender in a damping-integral tracking control structure.

In the remainder of the article, the experimental setup is defS.ExperimentalSetup, an electromechanical model is derived in Section III, open-loop performance is demonstrated in Section IV, the controller is designed in Section V, and conclusions are provided in Section VI.

II. EXPERIMENTAL SETUP

The piezoelectric bimorph actuator is a Y-poled T220-A4-503Y from Piezo Systems [13]. The dimensions are $63.5 \times 31.8 \times 0.51$ mm. It has a free displacement of ± 1 mm and a blocked force of ± 0.35 N. The internal construction is illustrated in Fig. 1. The layers include a 0.1 mm thick brass reinforcement layer shown in orange, two 0.2 mm thick piezoelectric plates shown in yellow, and two 5 μ m thick Nickel electrodes shown in blue. Fig. 1(a) illustrates the process used to create the integrated strain gauges. First, a 0.1 mm thick resin mask is printed on the electrode using a Form 2 Desktop 3D printer with 5 μ m resolution. Then 30% nitric acid is applied to etch the electrode area not covered by the mask. After removing the resin mask, the desired U-shaped feature, with an effective length of 40 mm and a width of 1 mm, is isolated from the rest of the electrode. This process is carried out on both the top and bottom electrodes. The U-shaped Nickel features are then employed as resistive metal foil strain gauges, while the rest of the electrode is used to drive the bender.

¹An earlier version of this paper was presented at the 2017 IEEE Sensors Conference and was published in its Proceedings. DOI: 10.1109/ICSENS.2017.8233951

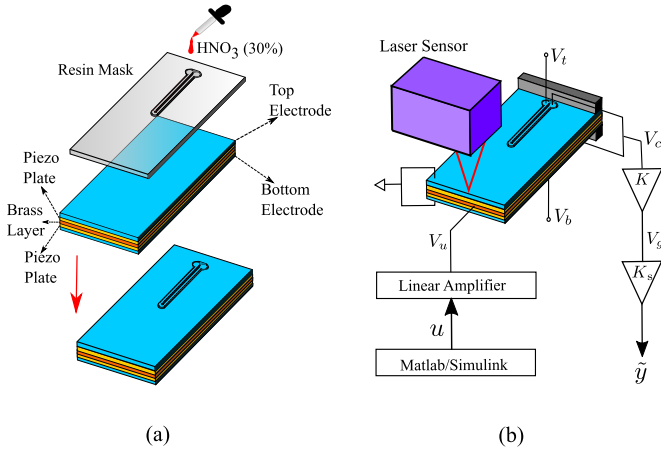


Fig. 1. Experimental setup. (a) Construction of strain gauges. (b) Experimentation procedure.

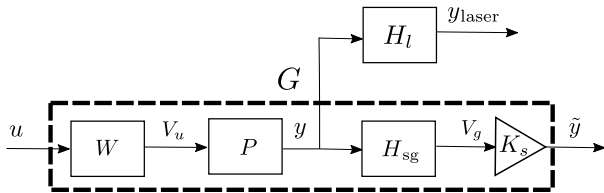


Fig. 2. Block diagram of the piezoelectric bender system with integrated strain sensors. The tip displacement of the bender is also measured using the laser (y_{laser}) for sensor calibration and comparison purposes.

Fig. 1(b) describes the experimental setup. The bender is cantilevered with a free length of 57 mm. It is driven in a parallel electrical configuration where the middle brass layer is grounded and a ± 90 V signal V_u is applied to the external electrodes using a PiezoDrive PD200 amplifier. It is noted that the strain gauges are isolated from V_u . An alternative configuration is to ground the external electrodes and drive the middle brass layer. However, as described in Appendix VI, this approach creates direct feed-through between the driving voltage and strain measurement, which is undesirable.

The strain gauges are excited in a half bridge configuration by applying a DC voltage to the top and bottom strain gauge V_t and V_b respectively. By tuning either V_t or V_b , the voltage at the center of the half bridge V_c can be set to zero. V_c is then amplified by a gain K , which provides a voltage V_g that is proportional to the tip displacement. The sensitivity K_s is found experimentally using the reference sensor. The estimated tip displacement is \tilde{y} in Fig. 1(b).

A block diagram of the setup is depicted in Fig. 2 where, W represents the linear amplifier dynamics, P represents the bender dynamics, H_l represents the laser dynamics, and H_{sg} represents the strain gauge dynamics. Therefore, the open-loop transfer function of the integrated bender is

$$G(s) = \frac{\tilde{y}}{u} = W(s)P(s)H_{sg}(s)K_s. \quad (1)$$

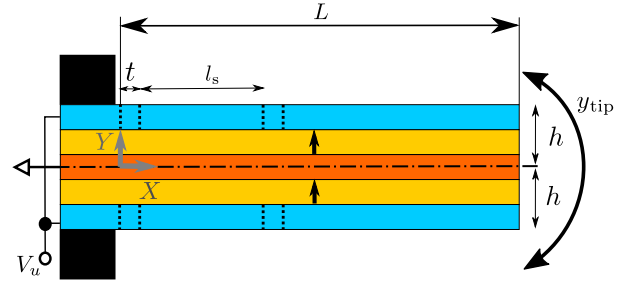


Fig. 3. Electromechanical model of the bender.

III. ELECTROMECHANICAL MODEL OF THE PIEZOELECTRIC BENDER

The proposed method uses the same principle as a resistive metal foil strain gauge. That is, the electrical resistance change is proportional to the surface strain. In benders, surface strain is also related to the tip displacement. Hence, the tip displacement of a bender can be estimated by measuring its surface resistance change. Subsection III-A derives a proportionality between surface strain and tip displacement. Subsection III-B relates the resistance change to tip displacement.

A. Tip Displacement and Surface Strain Relationship in Benders

In this study, Euler-Bernoulli beam theory is used. Tip displacement is considered to be relatively small, no external forces are exerted on the bender, and the driving voltage V_u is assumed to be effective across the thickness h of each piezoelectric plate. In Fig. 3, l_s is the nominal length of the strain gauges and t is a 0.5 mm gap which provides isolation from the high-voltage electrode. Using the constitutive equation for the inverse piezoelectric effect [14], the stress σ in each piezoelectric plate is,

$$\sigma = d_{31}E \frac{V_u}{h} + E\epsilon(x), \quad (2)$$

where, d_{31} is the piezoelectric constant, E is the Young's modulus, and $\epsilon(x)$ is the strain along the neutral axis. For relatively small tip displacements, $\epsilon(x)$ in (2) is replaced with $\epsilon(x) = -y \frac{d^2y}{dx^2}$, where y is the vertical distance from the neutral axis. The moment due to the external forces $M(x)$ can then be calculated by taking the integral of σy , over the cross-sectional area of the bender [4], that is

$$M(x) = d_{31}EV_u w \frac{h}{2} - EI \frac{d^2y}{dx^2}. \quad (3)$$

In (3), I is the moment of inertia and w is the width of the bender. Given that external forces are assumed to be absent, $M(x) = 0$, which simplifies (3) to,

$$\frac{d^2y}{dx^2} = d_{31}V_u w \frac{h}{2I}, \quad (4)$$

which indicates that the bender is experiencing a pure bending due to the applied driving voltage. Solving for y , at $x = L$, the tip displacement is,

$$y_{tip} = \frac{d_{31}V_u w h L^2}{2I}. \quad (5)$$

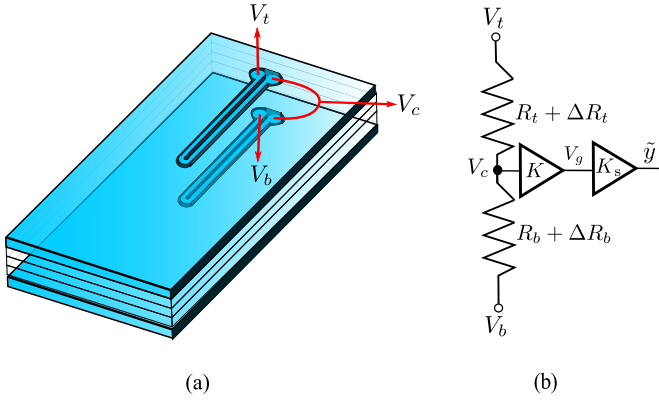


Fig. 4. The electrical connection of the strain gauges (a) and the equivalent circuit (b).

Using (4), the average surface strain $\epsilon_{ave,t}$ along the top sensor length l_s is

$$\epsilon_{ave,t} = \frac{1}{l_s} \int_t^{l_s+t} \epsilon(x) = \frac{-d_{31} V_u w h^2}{2I} \quad (6)$$

Comparing (5) with (6), the tip displacement y_{tip} and the average strain $\epsilon_{ave,t}$ are proportional. The proportionality is

$$\frac{y_{tip}}{\epsilon_{ave,t}} = -\frac{L^2}{2h}. \quad (7)$$

B. Surface Resistance Change Measurement

Fig. 4(a) illustrates the electrical connection of the integrated strain gauges. A conditioning circuit provides the top and bottom strain gauges with constant DC voltages of V_t and V_b . The equivalent circuit is shown in Fig. 4(b) where the nominal resistance of the top and bottom gauges is R_t and R_b respectively. When the bender moves, the top and bottom gauges experience a change in resistance ΔR_t and ΔR_b .

Assuming that the top and bottom sensors experience identical strain, $\epsilon_{ave} = \epsilon_{ave,t} = -\epsilon_{ave,b}$,

$$\epsilon_{ave} \propto \frac{\Delta R_t}{R_t} \propto \frac{\Delta R_b}{R_b}. \quad (8)$$

Using (7) and (8), the tip displacement can be estimated by measuring the resistance change, which is proportional to V_c . The excitation voltages V_t and V_b are tuned so that the nominal value of V_c is zero. When this is achieved, $\left(\frac{V_t}{V_b} = -\frac{R_t}{R_b}\right)$.

In the presence of strain, assuming that the strain gauges are identical ($R_t = R_b$), the voltage V_c is

$$V_c \propto \frac{\Delta R_t}{R_t} \propto \frac{\Delta R_b}{R_b}. \quad (9)$$

Using a gain of K , this voltage is amplified to $V_g = K V_c$. From equations (7-9),

$$V_g \propto y_{tip}. \quad (10)$$

The proportionality (10), is experimentally derived in the next section. The estimated displacement \tilde{y} is then

$$\tilde{y} = K_s V_g. \quad (11)$$

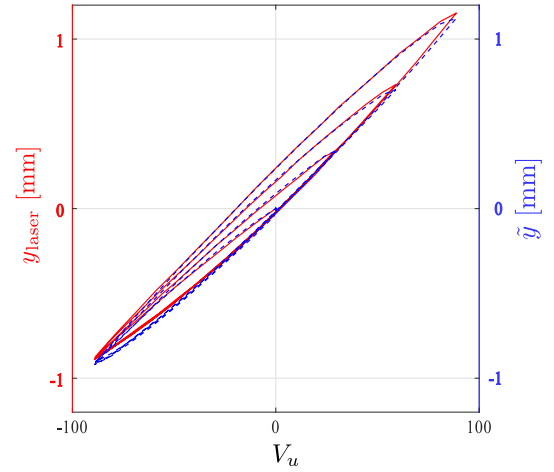


Fig. 5. The tip displacement versus driving voltage, when the actuator is driven by a triangular voltage with increasing amplitude.

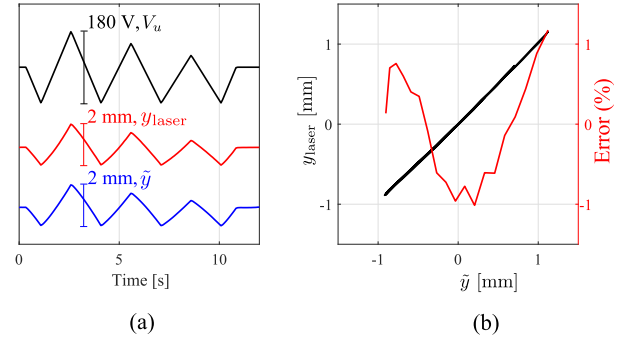


Fig. 6. The recorded time signals (a) and difference between the reference y_{laser} and proposed sensor \tilde{y} (b). In (a), the peak-to-peak values are provided for the actuator voltage V_u , the reference sensor y_{laser} , and strain sensor \tilde{y} .

IV. VALIDATION OF THE PROPOSED METHOD

A calibration experiment is first carried out where the maximum available driving voltage range $V_u = \pm 90$ V is applied to the bender and the tip displacement is measured using the laser sensor. The sensitivity gain is then calculated as $K_s = y_{laser} / V_g = 0.9$ mm/V.

The performance of the proposed strain sensor is further evaluated by applying a triangular driving voltage V_u to the actuator at 33%, 67%, and 100% of the full-scale voltage (± 90 V). The resulting tip displacements measured by both the reference and strain sensor are plotted in Fig. 5. The voltage-displacement hysteresis can be clearly observed in both signals.

Time signals are plotted in Fig. 6(a). A peak-to-peak driving voltage of 180 V results in a full-range of 2 mm of the displacement. A close agreement between the reference and strain sensor can be observed. In Fig. 6(b), the output of the reference and strain sensor are plotted against each other. The difference between the two sensors is calculated as a percentage of full-range, based on a least-squares fit for the sensitivity and offset. The maximum difference is 1.1 % of the full-range displacement. A polynomial calibration function could be used to significantly reduce the residual error.

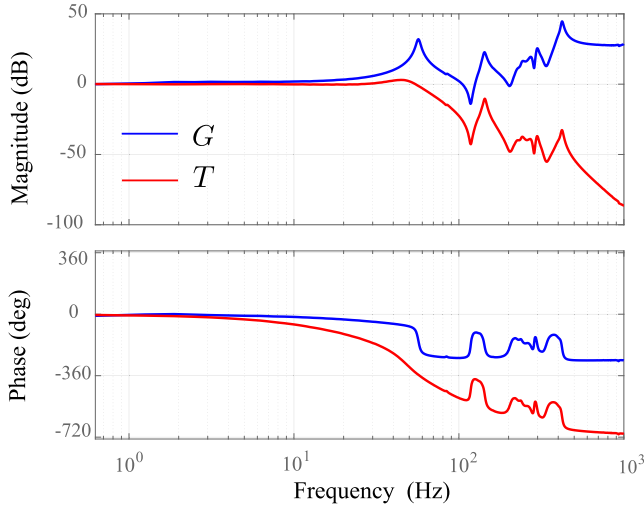


Fig. 7. The normalized open-loop frequency response in blue, measured from u to \tilde{y} , in mm/V. The closed-loop frequency response with damping-integral control, measured from r to \tilde{y} , in mm/V. Normalizing the open-loop frequency response is achieved by multiplying the measured data by a gain of 7.9.

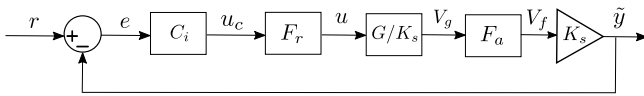


Fig. 8. Block diagram of the closed-loop system with the damping-integral controller. The strain sensor output is the measurement in the feedback loop.

V. CONTROLLER DESIGN

In this section the performance of the proposed strain sensor is evaluated in a closed-loop. A damping-integral controller [10] is designed and implemented in the feedback loop where the strain sensor measurement is used.

A. Damping-Integral Controller

The normalized open-loop frequency response from u to \tilde{y} , measured using a Quattro Data Physics signal analyzer, is plotted in Fig. 7. Investigating the frequency response, the first resonance occurs at 57 Hz. A damping-integral controller is designed to damp this resonance. Fig. 8 shows the block diagram of the closed-loop system with the damping-integral control strategy that includes an integral action

$$C_i = \frac{k_i}{s}, \quad (12)$$

a reconstruction filter F_r , and an anti-aliasing filter F_a . Both filters are second-order low pass Butterworth filters [10].

$$F_r = F_a = \frac{\omega_c}{s^2 + \sqrt{2}\omega_c s + \omega_c^2}. \quad (13)$$

The controller design criteria is to maximize the closed-loop bandwidth without destabilizing the closed-loop system [10]. The closed-loop transfer function is

$$T = \frac{C_i F_r F_a G}{1 + C_i F_r F_a G}. \quad (14)$$

TABLE I
PARAMETERS OF THE DAMPING-INTEGRAL CONTROLLER

Parameter	Value
ω_c	123 Hz
k_i	406

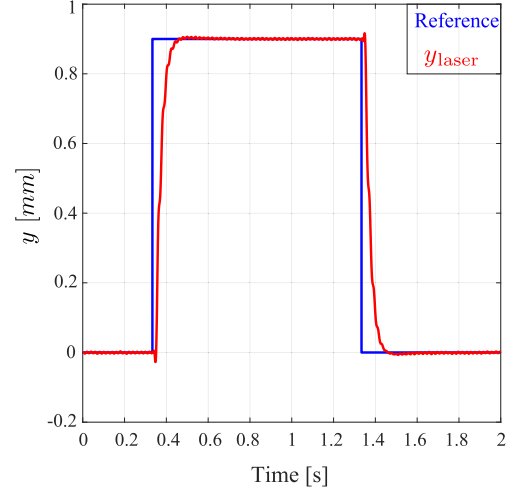


Fig. 9. Reference and measured closed-loop step response of the integrated bender using a damping-integral controller.

Employing the Nelder-Mead optimization algorithm [15], the cut-off frequency of the filters ω_c as well as the integral control gain k_i are optimized to fulfill the design criteria. The optimal parameters are summarized in Table I. The resultant loop gain and phase margin is 6 dB and 61° respectively.

B. Performance of the Closed-Loop System

The measured closed-loop frequency response of the bender with a damping-integral control is plotted on top of the open-loop frequency response in Fig. 7. It is observed that the first resonant peak is substantially suppressed by 33 dB and the resultant 3-dB closed-loop bandwidth of the system is 60 Hz.

The step response of the closed-loop system is plotted in Figure 9. A settling time of 0.06 s is recorded with no noticeable overshoot.

VI. CONCLUSION

The article presents a new method for measuring the tip displacement of piezoelectric benders by integrating resistive strain gauges into the top and bottom electrodes. The change in surface resistance is shown to be proportional to the tip displacement in the absence of external forces. The strain gauges are employed in a half bridge configuration to measure the resistance change and tip displacement.

The presented method is experimentally compared to a reference sensor. The maximum difference between the two sensor outputs was 1.1% of full range. The performance of the presented method for control applications is experimentally demonstrated by employing the method in a damping-integral

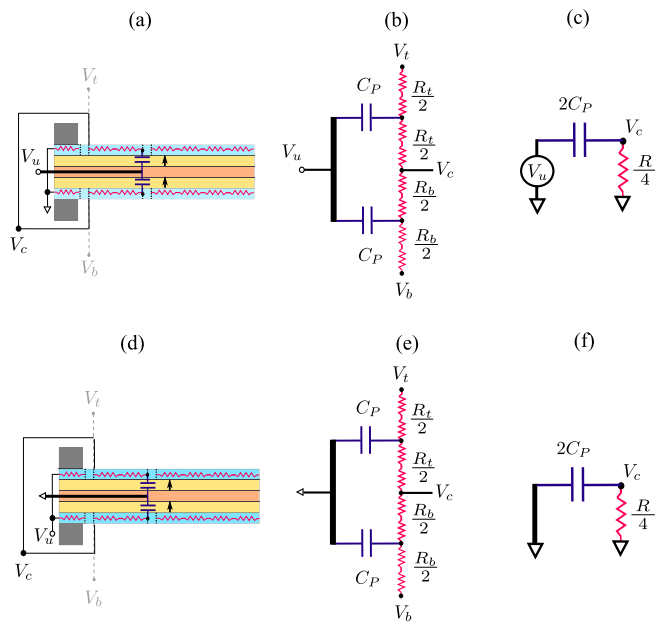


Fig. 10. Two electrical configurations for driving the bender. (a) Configuration 1. (b) Equivalent circuit. (c) Simplified circuit. (d) Configuration 2. (e) Equivalent circuit. (f) Simplified circuit.

control structure. The proposed sensing method has limitations for high frequency applications due to the capacitive coupling between the driven surface electrodes and the strain gauges, which is in the tens of kilohertz. Future work includes validating the high frequency performance of the proposed sensing method. The sensor geometry will also be optimized for external force measurement.

APPENDIX ELECTRICAL CONFIGURATION

Parallel poled benders, such as the Y-poled T220-A4-503Y bender, can be driven in two configurations:

- Configuration 1: The driving voltage V_u is applied to the middle brass layer and the external electrodes are ground.
- Configuration 2: The middle brass layer is grounded and V_u is applied to the external electrodes.

Configuration 1 is recommended by the manufacturer since it is convenient to have grounded external electrodes. However, this increases dynamic measurement errors. Figure 10 shows both configurations and their equivalent electrical circuits.

The electrical connections in Configuration 1 are described in Section II and depicted in Figure 10(a). The electrodes are grounded and V_u is applied to the middle layer. The top and bottom electrodes are electrically modeled as distributed resistances in series, while piezoelectric layers are modeled as distributed capacitances. The electrical equivalent circuit is described in Figure 10(b). Assuming that the resistances are equal, the simplified circuit in Figure 10(c) is a high-pass filter which allows direct feed-through from V_u to V_c at high frequencies, which is highly undesirable.

In Configuration 2, the equivalent circuit and simplified circuit is depicted in Figures 10(d) and (e) respectively. In this

configuration the direct feed-through is eliminated. In practice, there still exists a small capacitive coupling between the driven surface electrode and strain sensor; however, this is deemed to be negligible in the frequency range of interest.

ACKNOWLEDGMENT

The authors would like to thank Ben Routley for his assistance developing the etching process.

REFERENCES

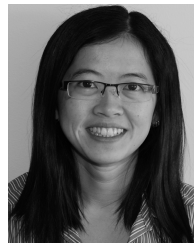
- [1] A. M. El-Sayed, A. Abo-Ismael, M. T. El-Melegy, N. A. Hamzaid, and N. A. A. Osman, "Development of a micro-gripper using piezoelectric bimorphs," *Sensors*, vol. 13, no. 5, pp. 5826–5840, 2013.
- [2] A. J. Fleming, "Nanopositioning system with force feedback for high-performance tracking and vibration control," *IEEE/ASME Trans. Mechatronics*, vol. 15, no. 3, pp. 433–447, Jun. 2010.
- [3] Y. K. Yong and A. J. Fleming, "High-speed vertical positioning stage with integrated dual-sensor arrangement," *Sens. Actuators A, Phys.*, vol. 248, pp. 184–192, Sep. 2016.
- [4] S. A. Rios and A. J. Fleming, "A new electrical configuration for improving the range of piezoelectric bimorph benders," *Sens. Actuators A, Phys.*, vol. 224, pp. 106–110, Apr. 2015.
- [5] P. Woias, "Micropumps—Past, progress and future prospects," *Sens. Actuators B, Chem.*, vol. 105, no. 1, pp. 28–38, Feb. 2005.
- [6] C. Jenke, J. P. Rubio, S. Kibler, J. Häfner, M. Richter, and C. Kutter, "The combination of micro diaphragm pumps and flow sensors for single stroke based liquid flow control," *Sensors*, vol. 17, no. 4, p. 755, 2017.
- [7] S. A. Rios and A. J. Fleming, "Design of a charge drive for reducing hysteresis in a piezoelectric bimorph actuator," *IEEE/ASME Trans. Mechatronics*, vol. 21, no. 1, pp. 51–54, Feb. 2016.
- [8] M. N. Islam and R. J. Seethaler, "Sensorless position control for piezoelectric actuators using a hybrid position observer," *IEEE/ASME Trans. Mechatronics*, vol. 19, no. 2, pp. 667–675, Apr. 2014.
- [9] J. L. Fanson and T. K. Caughey, "Positive position feedback control for large space structures," *AIAA J.*, vol. 28, no. 4, pp. 717–724, 1990.
- [10] A. A. Eielson, M. Vagia, J. T. Gravidahl, and K. Y. Pettersen, "Damping and tracking control schemes for nanopositioning," *IEEE/ASME Trans. Mechatronics*, vol. 19, no. 2, pp. 432–444, Apr. 2014.
- [11] S. S. Aphale, A. J. Fleming, and S. O. R. Moheimani, "Integral resonant control of collocated smart structures," *Smart Mater. Struct.*, vol. 16, no. 2, p. 439, 2007.
- [12] A. J. Fleming and K. K. Leang, "Integrated strain and force feedback for high-performance control of piezoelectric actuators," *Sens. Actuators A, Phys.*, vol. 161, nos. 1–2, pp. 256–265, Jun. 2010.
- [13] S. Z. Mansour, R. J. Seethaler, Y. R. Teo, Y. K. Yong, and A. J. Fleming, "Piezoelectric bimorph actuator with integrated strain sensing electrodes," in *Proc. IEEE SENSORS*, Oct./Nov. 2017, pp. 1–3.
- [14] D. A. Hall, "Review Nonlinearity in piezoelectric ceramics," *J. Mater. Sci.*, vol. 36, no. 19, pp. 4575–4601, Oct. 2001.
- [15] J. C. Lagarias, J. A. Reeds, M. H. Wright, and P. E. Wright, "Convergence properties of the Nelder–Mead simplex method in low dimensions," *SIAM J. Optim.*, vol. 9, no. 1, pp. 112–147, 1998.



Sepehr Zarif Mansour received the B.A.S. degree in mechanical engineering from the University of Tehran in 2013 and the M.A.S. degree in mechanical engineering from The University of British Columbia in 2015, where he is currently pursuing the Ph.D. degree in mechanical engineering. His research interests include the design and control of high-speed motion control systems.



Rudolf J. Seethaler (M'07) received the Ph.D. degree in mechanical engineering from The University of British Columbia (UBC), Vancouver, BC, Canada, in 1997. From 1997 to 2005, he was a Senior Controls Engineer for BMW AG, Munich, Germany. He is currently an Associate Professor with UBC. His research interests include the design and control of high-speed motion control systems.



Yuen Kuan Yong received the B.E. degree in mechatronics engineering and the Ph.D. degree in mechanical engineering from The University of Adelaide, Australia, in 2001 and 2007, respectively. She is currently an Associate Professor with The University of Newcastle, Australia. Her research interests include nanopositioning systems, design and control of micro-cantilevers, atomic force microscopy, and miniature robotics. She was a recipient of the University of Newcastle Vice-Chancellors Award for Research Excellence in 2014 and the Vice-Chancellors Award for Research Supervision Excellence in 2017. She is an Associate Editor of the IEEE/ASME TRANSACTIONS OF MECHATRONICS and *Frontiers in Mechanical Engineering*.



Yik R. Teo received the B.E.E. degree, the M.Phil. degree in mechanical engineering, and the Ph.D. degree from The University of Newcastle, Australia (Callaghan campus), in 2008, 2013, and 2018, respectively. He is currently a Research Associate with the Precision Mechatronics Laboratory, University of Newcastle. His research interests include high-precision positioning, scanning probe microscopy, and nanofabrication. Academic awards include the Glenn and Ken Moss Research Higher Degree Award, the Australian Postgraduate Award, and the Vice-Chancellor Award in Outstanding Research Candidate.



Andrew J. Fleming received the B.E.E. and Ph.D. degrees from The University of Newcastle, Australia (Callaghan campus), in 2000 and 2004, respectively. He is currently the Director of the Precision Mechatronics Laboratory, University of Newcastle. His research interests include lithography, nanopositioning, scanning probe microscopy, and biomedical devices. His research awards include the ATSE Baterham Medal in 2016, the IEEE Control Systems Society Outstanding Paper Award in 2007, and The University of Newcastle Researcher of the Year Award in 2007. He has co-authored three books and more than 180 journal and conference articles. He is the inventor of several patent applications. In 2012, he received the Newcastle Innovation Rising Star Award for Excellence in Industrial Engagement.